https://doi.org/10.15407/ufm.27.02.278

N.A. GURBANOV [1,*], Ch.A. IMAMALIZADE [1,], L.A. GARDASHOVA [1,***], M.M. YAŞAR [2,****], and A.H. GULIYEV [3,*****]**

[1] Azerbaijan State Oil and Industry University, 20 Azadlig Ave., Baku, Azerbaijan
[2] Karabuk University, 413 Ave., 10, 78050 Karabuk, Turkey
[3] Baku Engineering University, Khirdalan City, 120 Hasan Aliyev Ave., AZ0101 Baku, Azerbaijan

* nurlan.gurbanov@asoiu.edu.az, ** cimamelizade@gmail.com, *** l.qardashova@asoiu.edu.az, **** myasar@karabuk.edu.tr, ***** asquliyev@beu.edu.az

INVESTIGATION OF THE COMPOSITION–PHASE-TRANSFORMATION TEMPERATURE RELATIONSHIP IN THE NiTi-BASED ALLOYS USING MACHINE LEARNING

Accurate prediction of phase-transformation temperatures is crucial for the design and optimisation of NiTi-based shape-memory alloys, as these temperatures determine their functional performance and operating ranges. However, the relationship between alloy composition and phase-transformation behaviour is quite complex and nonlinear, making reliable prediction difficult, using conventional modelling approaches. Therefore, in this study, machine-learning methods are applied to predict the austenite final transformation temperature based on alloy composition. The dataset consists of experimentally measured NiTi-based alloys characterised by elemental atomic percentages and corresponding transformation temperatures. Before modelling, data preprocessing and feature standardisation are performed to ensure reliable model training and evaluation. Various regression methods, including ridge regression, support vector regression, Gaussian process regression, and k-nearest neighbours regression model, are applied and systematically compared. The results reveal that nonlinear ma-

Citation: N.A. Gurbanov, Ch.A. Imamalizade, L.A. Gardashova, M.M. Yaşar, and A.H. Guliyev, Investigation of the Composition–Phase-Transformation Temperature Relationship in the NiTi-Based Alloys Using Machine Learning, *Progress in Physics of Metals*, **27**, No. 2: 278–303 (2026)

chine-learning methods outperform significantly linear regression in capturing complex compositional dependences governing transformation temperatures. Specifically, nonparametric and probabilistic models demonstrate superior ability in modelling nonlinear relationships and experimental variability. The findings confirm that machine learning provides an effective and reliable framework for predicting transformation temperatures based solely on compositional parameters. The developed approach offers a valuable tool for accelerating data-driven design and optimisation of advanced shape-memory alloys, while reducing experimental effort and development time.

Keywords: shape-memory alloys, phase transformation, prediction model, machine learning, Python.

1. Introduction

Due to their behaviour governed by phase-transformation mechanisms, shape-memory alloys (SMAs) possess a range of unique functional properties [1]. It is precisely these characteristics that have attracted significant scientific and technological interest. In recent years, researchers have applied appropriate machine learning (ML) algorithms based on available experimental data and large databases and have proposed various computational models to predict the phase transformation temperatures of shape-memory alloys [2–6].

The predictive design of alloys within the process–structure–property–performance (PSPP) paradigm remains a highly complex and time-intensive task due to the multidimensional nature of alloy design and the governing physical mechanisms spanning atomic to macroscopic length scales 10^{-10}–10^{0} m and time scales from atomic vibrations to long-term degradation phenomena 10^{-14}–10^{7} s [1]. Major international initiatives, including Integrated Computational Materials Engineering (ICME) [2, 3] and the Materials Genome Initiative (MGI) [4], have demonstrated that combining physics-based simulations with data-driven methods can significantly accelerate the discovery and optimisation of advanced alloys. Particularly, machine learning (ML) techniques have proven effective in modelling PSPP relationships [5, 6], while also substantially reducing the number of costly experiments and simulations required for alloy development [7–9].

A key factor influencing ML performance in materials informatics is the formulation of effective descriptors through feature engineering. Many studies have focused on developing chemically and physically meaningful descriptors derived from high-throughput computational databases, such as AFLOW [10], OQMD [11], and Materials Project [12], which are often generated using density functional theory (DFT). These descriptor-driven approaches have enabled accurate prediction of diverse material properties, including glass-forming ability [13], band gap energies [14], formation enthalpies [15], crystal properties [16], superconducting critical temperatures [17, 18], and structural and electronic properties of Heusler

compounds and perovskites [19–21]. More recently, advanced thermodynamic descriptors incorporating entropy and enthalpy contributions, such as entropy density of states, have facilitated accelerated discovery of ultra-high-temperature ceramic materials [22]. Additionally, CALPHAD-based thermodynamic calculations have provided an efficient means to generate supplementary data for ML model development.

Despite these advances, most existing data-driven frameworks rely on large, well-structured datasets generated through computational methods, where data acquisition is relatively inexpensive. In contrast, experimental datasets are often limited in size and consistency due to variations in experimental methods, processing conditions, and data reporting standards. As a result, experimental databases typically contain only a limited number of observations for a given alloy system, often requiring decades of research to accumulate sufficient process–property data [23, 24]. This scarcity of experimental data presents a significant challenge for training robust ML models capable of accurately capturing complex nonlinear PSPP relationships.

Recent progress in alloy design has emphasised the importance of physics-informed feature engineering. Martin *et al.* [25] developed physically based quantitative metrics derived from crystallographic compatibility principles to identify phase combinations capable of minimising cracking during additive manufacturing. Their ML-assisted framework enabled rapid screening of thousands of crystallographic records and millions of potential phase combinations, significantly accelerating materials discovery. However, while ML efficiently automated the exploration of structural relationships, the subsequent optimisation of processing conditions and performance characteristics still required conventional materials engineering approaches. This highlights the need for more comprehensive ML frameworks capable of simultaneously integrating process, structure, and property relationships for accelerated alloy design.

Shape-memory alloys (SMAs) are a class of functional materials that exhibit unique thermomechanical properties, including the ability to recover their original shape after deformation and to display super-elastic behaviour under appropriate conditions [1, 26]. Owing to these remarkable characteristics, SMAs have found widespread applications in various engineering fields, including sensors, actuators, environmentally friendly refrigeration systems, and energy conversion technologies [27–29]. The functional performance of these materials is governed by reversible changes in their internal crystal structure, which occur within specific temperature intervals [30, 30]. As a result, the characteristic transformation temperatures define the operational temperature range and play a decisive role in determining the suitability of SMAs for practical applications [32–34]. In particular, the completion of the reverse phase transformation is essential for ensuring full shape recovery and achieving the desired functional response [35–37].

Among shape-memory alloys (SMAs), NiTi-based nitinol is one of the most extensively studied materials [36]. Nitinol is an intermetallic compound of the nickel–titanium system with a near-equiatomic composition (≅50 at.% Ni–50 at.% Ti) and is distinguished by its unique thermomechanical properties [35–38]. The functional behaviours observed in these materials, such as the shape-memory effect and superelasticity, are associated with solid-state phase transformations that occur during mechanical deformation and/or thermal cycling [38, 39].

When mechanical loading is applied to NiTi in the martensitic phase, the crystal structure consisting of twinned martensite transforms into a detwinned martensite configuration [36-38]. This transformation is governed by a diffusionless martensitic mechanism [39]. Subsequently, when the temperature of the material rises above the transformation temperatures, the crystal structure changes from martensite ($B19'$ monoclinic structure) to austenite ($B2$ b.c.c. structure), allowing the material to recover its pre-deformed shape [40, 41]. Upon subsequent cooling, the austenitic phase transforms back into twinned martensite, enabling the repeated manifestation of the shape-memory effect [41].

The transformation temperatures of NiTi-based alloys are highly sensitive to even small variations in chemical composition [33, 42]. In particular, an increase in titanium content leads to higher transformation temperatures, allowing the functional response of the material to be adjusted within a temperature range suitable for specific applications [43]. Conversely, increasing the nickel content lowers the transformation temperatures. Under such conditions, the material remains predominantly in the austenitic phase at room temperature, enabling the effective utilisation of the super-elastic (pseudo-elastic) behaviour of NiTi alloys [39–42]. This property is particularly important for applications such as biomedical implants, orthopaedic devices, and minimally invasive medical instruments [31, 36, 43].

One of the most widely used approaches for optimising the functional properties of NiTi-based shape-memory alloys is modification of the alloy composition [44]. Numerous studies have investigated the influence of adding ternary alloying elements to the base $Ti_{50}Ni_{50}$ system. These studies have demonstrated that the addition of such elements can significantly alter transformation temperatures while also improving the functional stability, thermomechanical behaviour, and cyclic durability of the material [34–45].

Liu *et al.* [46] developed a physics-informed machine-learning framework to predict transformation temperatures and hysteresis in NiTi and NiTiHf shape-memory alloys using a dataset combining literature and experimental records with detailed heat-treatment parameters. The study evaluated several regression models, including support vector Regression, random forest, and Gaussian process regression. Results showed that

physically informed feature engineering significantly improved prediction accuracy compared to using raw processing variables alone. Gaussian process regression demonstrated the best performance and provided uncertainty quantification, making it particularly suitable for reliable materials design and extrapolation.

Xue *et al.* [47] proposed a materials-informatics framework to predict martensitic transformation temperatures in NiTi-based alloys using a small, carefully controlled experimental dataset. The study identified three key physically meaningful descriptors-electronegativity, valence electron concentration, and atomic radius-related parameters as dominant predictors. Several regression methods were evaluated, with polynomial regression offering an optimal balance between accuracy and interpretability. The resulting surrogate model was integrated into an adaptive design loop to efficiently guide the discovery of new alloy compositions with targeted transformation properties.

Abedi *et al.* [48] developed a neural network model to predict multiple transformation temperatures (M_s, M_f, A_s, A_f) in NiTiHf alloys using combined composition and processing parameters. A curated dataset of 173 samples and twenty influential input features was used to train the model. The neural network achieved high predictive accuracy with an overall R^2 of approximately 0.92, demonstrating strong capability within the studied domain. The results confirmed the effectiveness of neural networks as a practical tool for accelerating alloy design and reducing experimental trial-and-error.

From a practical and engineering standpoint, the ability to predict accurately transformation temperatures based on alloy composition is essential for accelerating the development of advanced shape-memory alloys. In recent years, data-driven approaches and statistical learning methods have emerged as powerful tools for exploring complex compositional spaces and predicting material properties with high efficiency [49–52]. These materials informatics techniques have been successfully applied to a wide range of problems, including prediction of molecular properties, phase stability, structural classification, dielectric and piezoelectric properties, and electronic characteristics such as band gaps. Such approaches provide an effective framework for identifying compositional trends and enabling the rational design of shape-memory alloys with tailored transformation behaviour [53–55].

2. Data Selection and Modelling

2.1. Dataset Description

This dataset comprises 146 NiTi-based shape-memory alloy (SMA) compositions along with their experimentally measured phase transformation temperatures expressed in Kelvin [56–81] (Table 1). Each row represents

Table 1. **Chemical composition and phase transformation temperatures of NiTi-based shape-memory alloys [56–81]**

Alloys	M_f, K	M_s, K	A_s, K	A_f, K	Ref.
$Ni_{50}Ti_{49.9}Cr_{0.1}$	311.9	311.9	375.7	348.8	
$Ni_{50}Ti_{49.75}Cr_{0.25}$	276.5	302.6	348.9	323.6	
$Ni_{50}Ti_{49.5}Cr_{0.5}$	263.5	291.9	328.5	302.2	
$Ni_{50}Ti_{49.35}Cr_{0.65}$	260.1	284.4	316.3	296.1	
$Ni_{50}Ti_{49.2}Cr_{0.8}$	243.6	267.5	297.4	274.8	
$Ni_{50}Ti_{49}Cr_{1}$	214.8	237.3	268.3	252.1	
$Ni_{50}Ti_{48.75}Cr_{1.25}$	176.8	199.4	236.5	217.1	[56]
$Ni_{52.62}Ti_{47.09}Cr_{0.29}$	235	257	254	280	
$Ni_{50}Ti_{49.9}Cr_{0.1}$	323.8	323.8	323.8	323.8	
$Ni_{50}Ti_{49.75}Cr_{0.25}$	295.7	334.8	369.4	342.4	
$Ni_{50}Ti_{49}V_{1}$	284.1	318	347.7	327.3	
$Ni_{50}Ti_{48}V_{2}$	285.3	309	339.9	315.5	
$Ni_{50}Ti_{47}V_{3}$	270.7	292.5	317.5	300.3	
$Ni_{50}Ti_{45}V_{5}$	269	283.2	297	285.6	
$Ni_{50}Ti_{44}V_{6}$	261.1	279.1	294.5	281.8	
$Ni_{50.75}Ti_{49}V_{0.25}$	—	283	—	288	
$Ni_{50.5}Ti_{49}V_{0.5}$	—	278	—	281	
$Ni_{50}Ti_{49}V_{1}$	—	293	—	300	
$Ni_{50.875}Ti_{48.875}V_{0.25}$	—	276	—	281	
$Ni_{50.75}Ti_{48.75}V_{0.5}$	—	277	—	280	
$Ni_{50.5}Ti_{48.5}V_{1}$	—	276	—	279	[57]
$Ni_{51}Ti_{48.75}V_{0.25}$	—	273	—	278	
$Ni_{49.875}Ti_{49.875}V_{0.25}$	—	329	—	336	
$Ni_{49.75}Ti_{49.75}V_{0.5}$	—	330	—	335	
$Ni_{49.5}Ti_{49.5}V_{1}$	—	323	—	328	
$Ni_{48.75}Ti_{48.75}V_{2.5}$	—	303	—	308	
$Ni_{48}Ti_{48}V_{4}$	—	294	—	299	
$Ni_{48.75}Ti_{50.75}V_{0.5}$	—	336	—	341	
$Ni_{50}Ti_{49.5}V_{0.5}$	—	308	—	343	
$Ni_{50.25}Ti_{49.25}V_{0.5}$	—	288	—	293	
$Ni_{49.8}Ti_{48.2}Hf_{2}$	317.2	355.6	394.7	358.3	
$Ni_{49.8}Ti_{46.2}Hf_{4}$	325.5	358.8	406.8	368.5	
$Ni_{49.8}Ti_{44.2}Hf_{6}$	329	363.9	421.4	381.3	
$Ni_{49.8}Ti_{42.2}Hf_{8}$	355.9	384.1	448.3	418.1	
$Ni_{49.8}Ti_{40.2}Hf_{10}$	377.7	401.1	464.8	438.4	[56]
$Ni_{49.8}Ti_{39.2}Hf_{11}$	389.8	414.9	475.9	449	
$Ni_{49.8}Ti_{35.95}Hf_{14.63}$	380	460	435	510	

Continuation of the Table 1

Alloys	M_f, K	M_s, K	A_s, K	A_f, K	Ref.
$Ni_{49.8}Ti_{35.2}Hf_{15}$	451	480	530.9	512	
$Ni_{49.8}Ti_{30.2}Hf_{20}$	546.4	573.1	610.6	595.8	
$Ni_{50}Ti_{32}Hf_{18}$	468	499	505	536	[58]
$Ni_{49}Ti_{36}Hf_{15}$	421	452	489	504	[59]
$Ni_{50}Ti_{38}Hf_{12}$	380	405	430	450	
$Ni_{50}Ti_{35}Hf_{15}$	430	450	480	500	[60]
$Ni_{50}Ti_{30}Hf_{20}$	495	520	564	585	
$Ni_{45}Ti_{50}Pd_{5}$	307.7	328.5	355.2	335.2	
$Ni_{43}Ti_{50}Pd_{7}$	302.3	323.3	347.1	331.3	
$Ni_{41}Ti_{50}Pd_{9}$	322.3	329.4	341.3	331.2	
$Ni_{39}Ti_{50}Pd_{11}$	318.2	335.7	347.6	334.7	
$Ni_{37}Ti_{50}Pd_{13}$	332.1	348.5	365.3	352.8	[56]
$Ni_{35}Ti_{50}Pd_{15}$	351.3	364.9	377.5	367.2	
$Ni_{33}Ti_{50}Pd_{17}$	365.9	383.2	397.3	385.6	
$Ni_{29}Ti_{50}Pd_{21}$	406.4	424.5	440.3	426.6	
$Ni_{20}Ti_{50}Pd_{30}$	515.3	533.8	546.8	534.9	
$Ni_{34.5}Ti_{50.5}Pd_{15}$	338	346	348	356	
$Ni_{29.5}Ti_{50.5}Pd_{20}$	396	405	406	416	
$Ni_{24.5}Ti_{50.5}Pd_{25}$	451	463	466	470	[61]
$Ni_{24.7}Ti_{50.3}Pd_{25}$	454	465	468	474	[62]
$Ni_{19.5}Ti_{50.3}Pd_{30}$	506	522	523	532	[61]
$Ni_{16}Ti_{54}Pd_{30}$	481	513	509	546	
$Ni_{6}Ti_{54}Pd_{40}$	628	664	674	726	[63]
$Ni_{3}Ti_{54}Pd_{43}$	648	720	725	789	
$Ni_{3.5}Ti_{50.5}Pd_{46}$	742	758	782	786	[61]
$Ni_{49.5}Ti_{49.5}Zr_{1}$	322.3	353.2	388.9	358.3	
$Ni_{49.5}Ti_{47.5}Zr_{3}$	313.2	345.9	395.8	355.6	
$Ni_{49.5}Ti_{45.5}Zr_{5}$	304.2	338.7	401.6	352.4	[53]
$Ni_{52}Ti_{42}Zr_{6}$	196	197	240	312	
$Ni_{49.5}Ti_{40.5}Zr_{10}$	344.6	372.4	428.2	401.8	
$Ni_{49.5}Ti_{35.5}Zr_{15}$	435.2	464	505.9	483.4	
$Ni_{48.78}Ti_{33.01}Zr_{18.21}$	410	490	470	550	[64]
$Ni_{49.5}Ti_{30.5}Zr_{20}$	535.7	560.4	606.4	584.7	[56]
$Ni_{50}Ti_{32}Zr_{18}$	372	401	412	432	[55]
$Ni_{50}Ti_{44}Zr_{6}$	—	—	354	373	[65]
$Ni_{50}Ti_{38}Zr_{12}$	—	—	369	415	[66]
$Ni_{50}Ti_{32}Zr_{18}$	—	—	394	445	
$Ni_{50}Ti_{26}Zr_{24}$	—	—	593	688	[65]

Continuation of the Table 1

Alloys	M_f, K	M_s, K	A_s, K	A_f, K	Ref.
$Ni_{34.5}Ti_{50}Pt_{15.5}$	452	479	475	495	
$Ni_{34.0}Ti_{50}Pt_{16.0}$	460	486	477	499	[67]
$Ni_{33.5}Ti_{50}Pt_{16.5}$	480	492	495	504	
$Ni_{28.5}Ti_{50.5}Pt_{21}$	548.3	597.6	626.2	585.5	[56]
$Ni_{28}Ti_{52}Pt_{20}$	565	504	549	609	
$Ni_{30}Ti_{50}Pt_{20}$	548	491	537	588	[58]
$Ni_{32}Ti_{48}Pt_{20}$	574	539	592	624	
$Ni_{26}Ti_{54}Pt_{20}$	597	634	646	695	[63]
$Ni_{51.4}Ti_{44.8}Cu_{3.8}$	223	273	263	303	[54]
$Ni_{43}Ti_{52}Cu_{5}$	307.1	327.7	355.4	337	
$Ni_{43.5}Ti_{51.5}Cu_{5}$	313.6	333.4	358.8	342.4	
$Ni_{44}Ti_{51}Cu_{5}$	311.3	333	360.4	341.1	
$Ni_{44.2}Ti_{50.7}Cu_{5}$	312.6	333.5	356.5	337.4	
$Ni_{44.5}Ti_{50.5}Cu_{5}$	309.2	332.8	358.1	337.4	
$Ni_{44.6}Ti_{50.4}Cu_{5}$	316.3	338.4	360.7	341.1	
$Ni_{44.75}Ti_{50.25}Cu_{5}$	324.3	341.8	362.9	346.2	
$Ni_{45}Ti_{50}Cu_{5}$	316.7	344.7	367.7	339.6	
$Ni_{45.2}Ti_{49.8}Cu_{5}$	301.7	326.6	350.7	328.3	
$Ni_{45.3}Ti_{49.7}Cu_{5}$	299.3	318.4	339.6	320.7	[56]
$Ni_{45.7}Ti_{49.3}Cu_{5}$	284.4	303.8	329.8	313	
$Ni_{45.9}Ti_{49.1}Cu_{5}$	270.6	288.8	311.5	294.6	
$Ni_{46.0}Ti_{49.0}Cu_{5}$	257.3	271.5	288.6	278.3	
$Ni_{46.1}Ti_{48.9}Cu_{5}$	241.5	261.9	285.3	266.1	
$Ni_{46.2}Ti_{48.8}Cu_{5}$	234.1	250.9	272.3	259.7	
$Ni_{47.5}Ti_{50}Cu_{2.5}$	224.4	240.3	259.2	244	
$Ni_{42.5}Ti_{50}Cu_{7.5}$	317.9	344.6	380.2	354.2	
$Ni_{41}Ti_{49}Cu_{10}$	319.7	337	356.9	342.7	
$Ni_{40}Ti_{50}Cu_{10}$	280.6	302.8	307.5	323	[69]
$Ni_{41.5}Ti_{48.5}Cu_{10}$	293.9	314.4	325.7	339.6	
$Ni_{45}Ti_{50}Cu_{5}$	287.4	310.5	325.7	333	
$Ni_{40}Ti_{50}Cu_{10}$	295	309	311	330	[70]
$Ni_{47.5}Ti_{50}Cu_{12.5}$	179	292	192	300	
$Ni_{49}Ti_{46}Nb_{5}$	170	280	180	286	
$Ni_{49.5}Ti_{45.5}Nb_{5}$	173	233	265	290	[71]
$Ni_{49.8}Ti_{45.2}Nb_{5}$	117	195	220	265	
$Ni_{50}Ti_{45}Nb_{5}$	98	167	197	242	
$Ni_{50}Ti_{48}Nb_{2}$	88	117	186	221	
$Ni_{49.6}Ti_{45.9}Nb_{4.5}$	279	289	311	338	

The End of the Table 1

Alloys	M_f, K	M_s, K	A_s, K	A_f, K	Ref.
$Ni_{49.8}Ti_{45.2}Nb_5$	178	196	225	262	[72]
$Ni_{47}Ti_{44}Nb_9$	133	173	208	255	
$Ni_{46.8}Ti_{48.7}Nb_{4.5}$	183	200	248	262	[66]
$Ni_{50}Ti_{49}Nb_1$	265	285	310	325	
$Ni_{50}Ti_{47}Nb_3$	—	323	348	373	[73]
$Ni_{50.7}Ti_{49.3}Ce_0$	—	230	262	300	
$Ni_{50.45}Ti_{49.05}Ce_{0.5}$	207	226.5	235	249	
$Ni_{50.2}Ti_{48.8}Ce_1$	291	298.5	321	344	[74]
$Ni_{49.7}Ti_{48.3}Ce_2$	301	321	339	364.5	
$Ni_{46.8}Ti_{48.2}Ce_5$	331	338	364	373	
$Ni_{50.7}Ti_{49.3}Dy_0$	341	350	374	387	
$Ni_{50.2}Ti_{48.8}Dy_1$	226	207	235	249	[75]
$Ni_{45.7}Ti_{44.3}Dy_{10}$	313	290	315	347	
$Ni_{50.7}Ti_{49.3}La_0$	337	320	367	374	
$Ni_{50.2}Ti_{48.8}La_1$	207	226	235	249	[76]
$Ni_{50}Ti_{49}Y_1$	272	288	313	316	
$Ni_{50}Ti_{48}Y_2$	325	273	333	373	[77]
$Ni_{50}Ti_{40}Y_{10}$	335	297	351	378	
$Ni_{47.6}Ti_{50}Fe_{2.4}$	300	288	319	330	
$Ni_{47}Ti_{50}Fe_3$	168	213	265	223	[78]
$Ni_{46.6}Ti_{50}Fe_{3.4}$	113	173	203	168	
$Ni_{50}Ti_{49}Sc_1$	77	133	113	163	
$Ni_{50}Ti_{49.99}Sc_{0.01}$	293	331	333	373	
$Ni_{50}Ti_{48}Sc_2$	353	393	393	398	[77]
$Ni_{50}Ti_{45}Sc_5$	264	293	313	340	
$Ni_{51}Ti_{48.5}Sc_{0.5}$	77	133	153	183	
$Ni_{49}Ti_{51}Si_0$	163	263	258	280	
$Ni_{48}Ti_{51}Si_1$	316	348	345	371	[79]
$Ni_{47}Ti_{51}Si_2$	320	355	348	387	
$Ni_{50}Ti_{47}Ta_3$	314	331	363	379	[80]
$Ni_{49}Ti_{46}Ta_5$	314	328	350	373	
$Ni_{50}Ti_{45}Ta_5$	304	317	349	372	[81]

an individual alloy identified by an ‘Alloy’ label, while the dataset contains 146 columns in total, including 16 features corresponding to the atomic percentages (at.%) of the constituent elements-Ni, Ti, and possible alloying additions such as Cr, V, Hf, Pd, Zr, Pt, Cu, Nb, Ce, Dy, La, Y, Fe, Sc, Si, and Ta, with non-present elements recorded as zero and four output

variables describing the characteristic transformation temperatures (martensite start transformation temperature, M_s, martensite finish transformation temperature, M_f, austenite start transformation temperature, A_s, and austenite finish transformation temperature, A_f) that capture both forward martensitic and reverse austenitic transformations. The alloys cover multiple compositional families with distinct metallurgical trends, including temperature-depressing systems (NiTi–Cr/V), high-temperature-enhancing systems (NiTi-Hf/Pd/Zr/Pt), and various modifications based on Cu, Nb, rare-earth elements, Fe, Sc, Si, and Ta, thereby enabling comparative analysis across chemically different dopant classes. Some entries contain missing temperature values, and numerical formatting may use decimal commas, requiring appropriate pre-processing such as type conversion, normalisation, and missing-data handling prior to modelling. Overall, the dataset is well suited for supervised regression, sensitivity analysis, and feature-importance studies aimed at quantifying the influence of compositional variations on phase transformation behaviour in NiTi-based SMAs.

2.2. Software Supply

The computational work was carried out using Python 3.14, with all analyses implemented in the Jupyter Notebook environment (an interactive, browser-based platform built on Python). Jupyter Notebook was selected to facilitate rapid and transparent development of the data-processing and modelling workflow, enabling step-by-step execution of code, immediate visualisation of intermediate results, and straightforward documentation of procedures alongside the computations [82, 83]. This setup supports efficient exploratory analysis and reproducible research practices, when working with the presented dataset.

2.3. Data Pre-Processing

The dataset was divided into input features (X) and target output (y). The input matrix consisted of the first 17 columns representing the atomic percentages (at.%) of alloying elements, which describe the chemical composition of each NiTi-based shape-memory alloy. The austenite finish temperature (A_f) was selected as the regression target, as this parameter plays a critical role in determining the functional behaviour and activation temperature of the shape-memory effect. From an application perspective, A_f directly defines the temperature, at which the alloy fully recovers its original shape, making it the most relevant design parameter for engineering purposes. Consequently, predicting A_f from composition enables efficient data-driven optimisation and design of new shape-memory alloys.

To evaluate the predictive capability of the developed models, the dataset was randomly divided into training and testing subsets. Specifically,

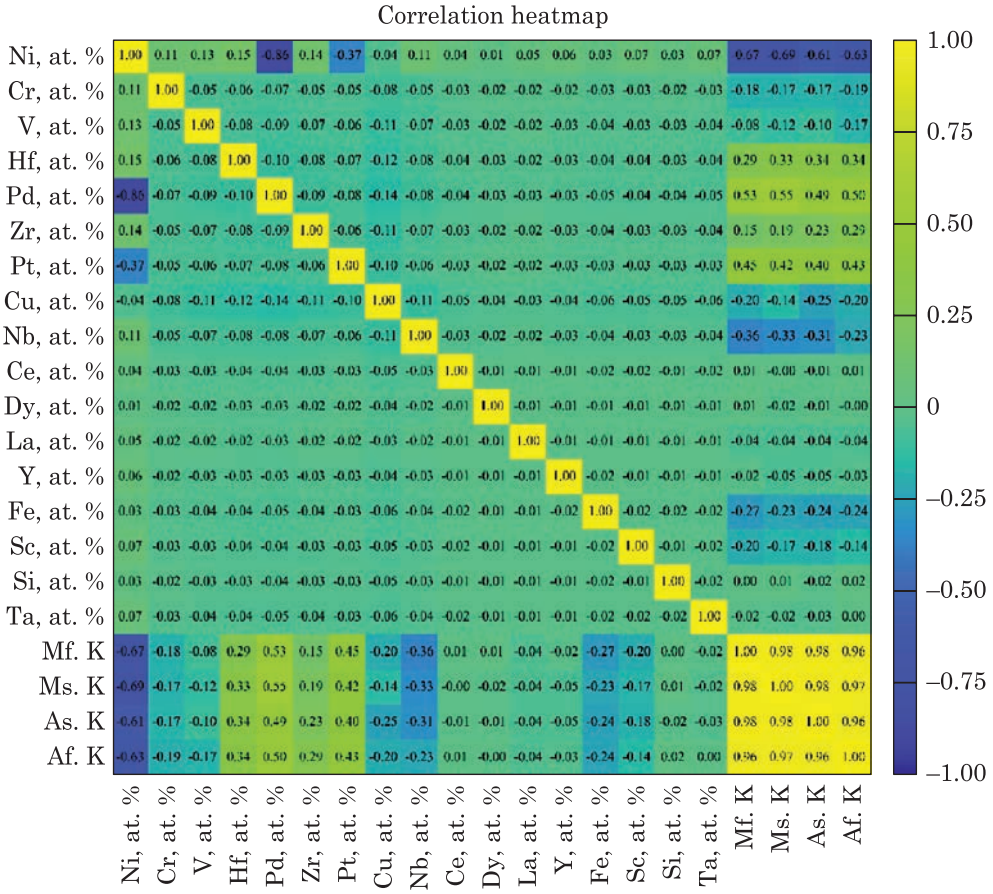

Fig. 1. Correlation relationship between features

80% of the data were allocated to the training set (X_train, y_train) for model fitting, while the remaining 20% constituted the testing set (X_test, y_test) for independent performance evaluation. This split ratio is commonly adopted in machine learning studies as it provides a balanced trade-off between sufficient data for model learning and reliable validation on unseen samples. Such separation allows assessment of both training accuracy and generalisation performance, thereby reducing the risk of overfitting and ensuring that the model predictions remain robust for new alloy compositions.

Before model training, feature standardisation was performed using the Standard Scaler method. The scaler parameters (mean and standard deviation) were computed exclusively on the training set to prevent data leakage. Subsequently, both training and test sets were transformed using the same scaling parameters. This procedure ensures realistic model evaluation and avoids artificially inflated performance.

The correlation matrix (Fig. 1) reveals several meaningful trends between alloy composition and transformation temperatures. Among the compositional variables, Ni exhibits a strong negative correlation with all transformation temperatures ($r = -0.61$ to -0.69), indicating that increasing Ni content depresses the martensitic and austenitic transformation temperatures. In contrast, Pd shows a pronounced positive correlation ($r = 0.49–0.55$), confirming its well-known role as a high-temperature stabilising element. Moderate positive correlations are observed for Hf, Pt, and Zr ($r \cong 0.15–0.45$), suggesting a secondary contribution to temperature elevation. Most of the remaining alloying elements demonstrate weak or near-zero linear correlations ($|r| < 0.1$), implying limited pair-wise linear influence. Additionally, a strong inverse correlation between Ni and Pd ($r = -0.86$) indicates compositional interdependence and potential multicollinearity. Finally, the transformation temperatures themselves are highly correlated with each other ($r > 0.96$), reflecting their common thermodynamic origin.

However, it should be emphasised that correlation analysis reflects only linear pair-wise relationships and therefore cannot fully capture the complex, nonlinear, and interaction-driven effects that govern multicomponent NiTi-based shape-memory alloys. In practice, transformation temperatures are often influenced by synergistic contributions of multiple elements and higher-order interactions that are not detectable through simple correlation coefficients. Consequently, eliminating features solely based on low correlation values may lead to the loss of potentially informative variables. For this reason, all sixteen compositional parameters were retained as input features in the subsequent modelling stage to ensure that both linear and nonlinear dependences are preserved and to maximise the predictive capability of the machine learning models.

2.4. Model Evaluation Metrics

To evaluate quantitatively the predictive performance of the developed regression model, two widely used statistical metrics were employed: root mean square error (RMSE) and the coefficient of determination (R^2) [84, 85].

The RMSE measures the average magnitude of prediction errors and is defined as [84]

$$\mathrm{RMSE} = \sqrt{\sum_{i=1}^{n} \left(y_i - \widehat{y}_i\right)^2}\ , \qquad (1)$$

where y_i represents the experimentally measured value, $\widehat{y}_i$ represents the predicted value obtained from the model, and n is the total number of samples. RMSE provides an estimate of the standard deviation of prediction errors and is expressed in the same units as the target variable. Lower RMSE values indicate higher prediction accuracy [84, 85].

The coefficient of determination R^2 evaluates how well the model explains the variance in the target variable and is defined as [84]

$$R^2 = 1 - \sum_{i=1}^{n} \left(y_i - \hat{y}_i\right)^2 \Big/ \sum_{i=1}^{n} \left(y_i - \overline{y}_i\right)^2, \quad (2)$$

where $\overline{y}_i$ is the mean of the observed values. The R^2 metric ranges from 0 to 1, where values closer to 1 indicate better predictive performance and stronger agreement between predicted and experimental values. Both RMSE and R^2 were calculated for the training and test datasets to evaluate model accuracy and generalisation capability [84].

3. Results and Discussions

To establish a baseline reference, ridge regression was first implemented as a regularised linear regression model [85, 86]. This method provides a stable and interpretable framework for modelling the relationship between alloy composition and transformation temperature by introducing a regularisation term that reduces coefficient instability and improves numerical robustness [84]. However, due to its linear formulation, ridge regression has limited capability to capture complex nonlinear interactions between alloying elements (as it is in realistic systems with long-range interatomic interactions, which include contributions in all co-ordination shells [87–96]) and the A_f transformation temperature. To ensure reliable and reproducible model performance, hyperparameter optimisation was performed using GridSearchCV combined with 5-fold cross-validation (shuffle = True, random_state = 42). The ridge regression model applies *L2* regularisation controlled by the regularisation parameter α, which determines the strength of coefficient penalisation and directly affects model bias–variance balance. The hyperparameter α was systematically optimised over a logarithmically spaced range α Î [0.001, 100], ensuring objective and comprehensive exploration of model configurations. The optimal hyperparameter value was selected based on cross-validation error minimisation using mean squared error as the optimisation criterion. The final model was then used to generate predictions for both training and test datasets, and performance was evaluated using RMSE and R^2, ensuring robust model selection, reliable prediction accuracy, and full reproducibility of the regression procedure. As a result, the model demonstrated the lowest predictive accuracy among the considered approaches shown in. Specifically, the model achieved an RMSE of 40.8501 K and an R^2 value of 0.8734 on the training set (Fig. 2, *a*), while on the test set it achieved an RMSE of 37.9149 K and an R^2 value of 0.8970 (Fig. 2, *b*). Although these results indicate that the model was able to capture the general trend in the data, the relatively high prediction error suggests that linear regression is insufficient for accurately modelling the underlying physical relationships governing transformation temperature [4, 73].

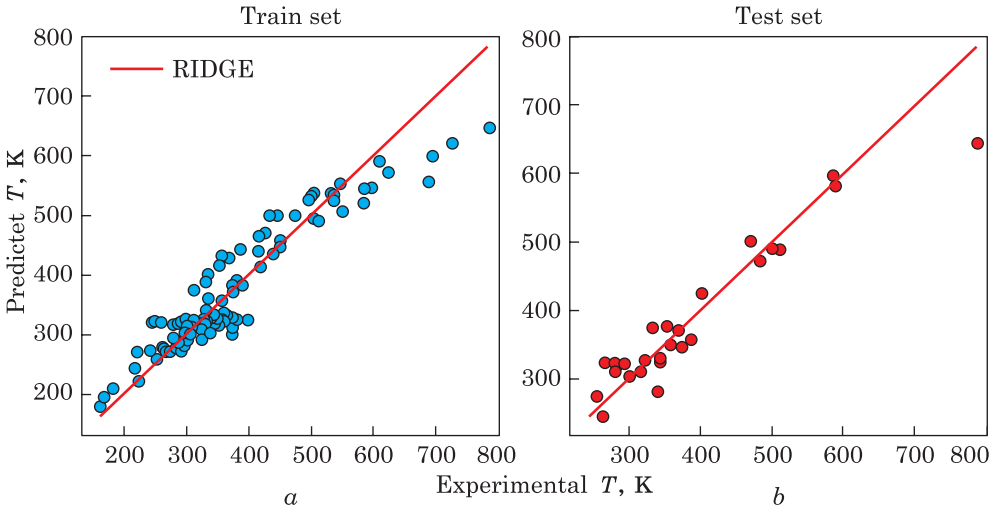

Fig. 2. Model evaluation results of ridge method

To overcome the limitations of linear modelling, the support vector regression (SVR) model with a nonlinear kernel was implemented [97]. Unlike linear regression, SVR is capable of modelling nonlinear relationships by transforming the input space into a higher-dimensional feature space, allowing more flexible approximation of complex dependences [54, 55]. To ensure robust and reproducible predictive performance, hyperparameter optimisation was conducted using GridSearchCV in combination with 5-fold cross-validation (shuffle = True, random_state = 42). Before model training, all input features were standardised using StandardScaler to achieve zero mean and unit variance, which is essential for the stable and reliable performance of kernel-based methods such as SVR. Data preprocessing and regression modelling were integrated within a unified Pipeline framework to ensure consistent transformation during training, validation, and testing, while preventing data leakage [4]. The SVR hyperparameters were systematically tuned over predefined ranges, including the regularisation parameter $C \in \{1, 10, 50, 100, 500\}$, kernel coefficient $\gamma \in \{\text{scale}, 0.001, 0.01, 0.05, 0.1\}$, and epsilon parameter $\epsilon \in \{0.05, 0.1, 0.2, 0.3\}$. The optimal hyperparameter combination was selected based on cross-validation error minimisation, and the final model performance was assessed using RMSE and R^2 on both training and test datasets, ensuring reliable model selection, improved predictive accuracy, and full reproducibility of the optimisation process. The SVR model demonstrated a significant improvement in predictive accuracy compared to ridge regression. On the training set, the model achieved an RMSE of 28.7488 K and an R^2 value of 0.9373 (Fig. 3, *a*), while on the test set, it achieved an RMSE of 34.2882 K and an R^2 value of 0.9157 (Fig. 3, *b*). These results indicate

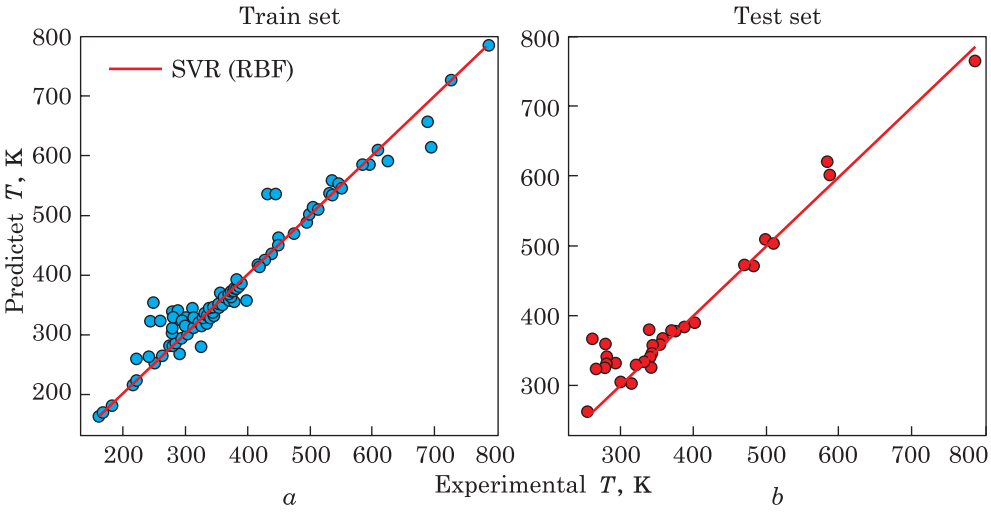

Fig. 3. Model evaluation results of SVR (RBF) method

that the nonlinear structure of SVR allows it to capture better the relationship between alloy composition and transformation temperature, leading to improved predictive performance and generalisation capability.

To improve further prediction accuracy, Gaussian process regression (GPR) was implemented [98]. This method provides a highly flexible probabilistic framework that can model complex nonlinear relationships while explicitly accounting for uncertainty and noise present in experimental data [62]. Unlike deterministic regression methods, GPR defines a distribution over possible functions, allowing it to adapt effectively to intricate patterns in the dataset. For this probabilistic framework, model configuration was determined using the same systematic optimization strategy employed in the previous regression models, namely GridSearchCV combined with 5-fold cross-validation (shuffle = True, random_state = 42), thereby ensuring methodological consistency, objective model selection, and full reproducibility across all considered approaches. Unlike ridge regression and SVR, where optimisation primarily involves tuning regularisation-related parameters, the performance of GPR is fundamentally governed by the choice of covariance kernel, which defines the smoothness, flexibility, and noise characteristics of the regression function. Candidate kernels included Constant×RBF + WhiteKernel and Constant×Matern + + WhiteKernel formulations, allowing the model to represent different functional behaviours and levels of stochastic variability. The kernel hyperparameters were explored over predefined ranges, including length scale $l \in [0.3, 3.0]$, noise level $\sigma \in [10^{-4}, 10^{-1}]$, and Matern smoothness parameter $\nu \in \{0.5, 1.5, 2.5\}$. The inclusion of WhiteKernel enables explicit modelling of observational noise, which is particularly important when

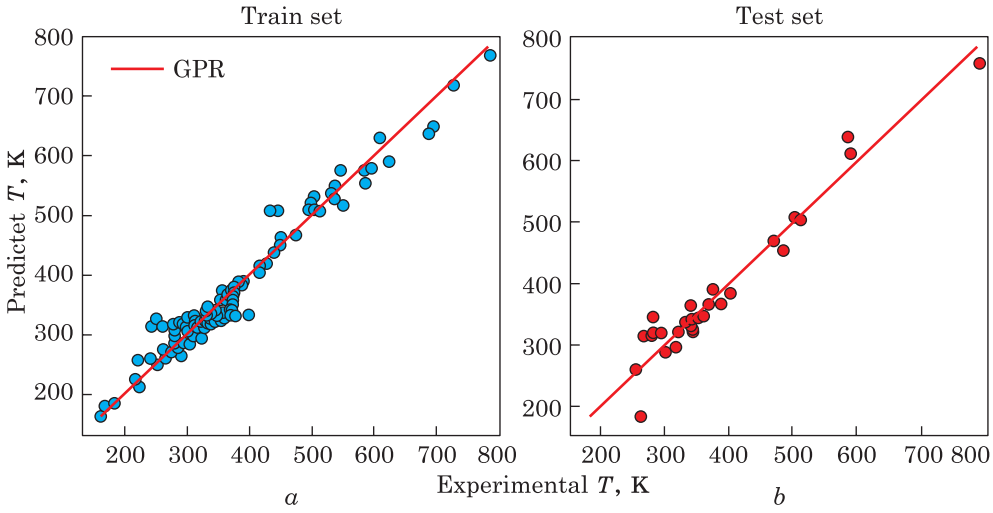

Fig. 4. Model evaluation results of GPR method

working with experimentally measured transformation temperatures. The optimal kernel structure was selected based on cross-validation error minimisation, and the final model was evaluated using RMSE and coefficient of determination R^2, ensuring reliable probabilistic prediction, improved generalisation performance, and full reproducibility of the modelling procedure. The GPR model demonstrated superior predictive performance compared to both ridge regression and SVR. The training set results showed an RMSE of 26.0444 K and an R^2 value of 0.9485 (Fig. 4, *a*), while the test set results showed an RMSE of 29.2709 K and an R^2 value of 0.9386 (Fig. 4, *b*). These results indicate that GPR provides more accurate and robust predictions by effectively capturing nonlinear dependences and accommodating experimental variability.

Finally, the *k*-nearest neighbours (KNN) regression model was implemented as a non-parametric machine learning method that predicts transformation temperature based on similarity between alloy compositions [98–101]. Unlike parametric models, KNN does not assume a predefined functional relationship between input and output variables [100]. Instead, predictions are made based on local relationships within the data, allowing the model to capture effectively highly nonlinear and complex dependences [102–105]. Importantly, to maintain methodological consistency across all machine-learning models considered in this study, the KNN model was optimised using the same hyperparameter tuning framework employed in the previous methods, namely GridSearchCV combined with 5-fold cross-validation (shuffle = True, random_state = 42). This unified optimisation strategy ensures objective comparison, consistent validation conditions, and full reproducibility of the modelling procedure. Since KNN perfor-

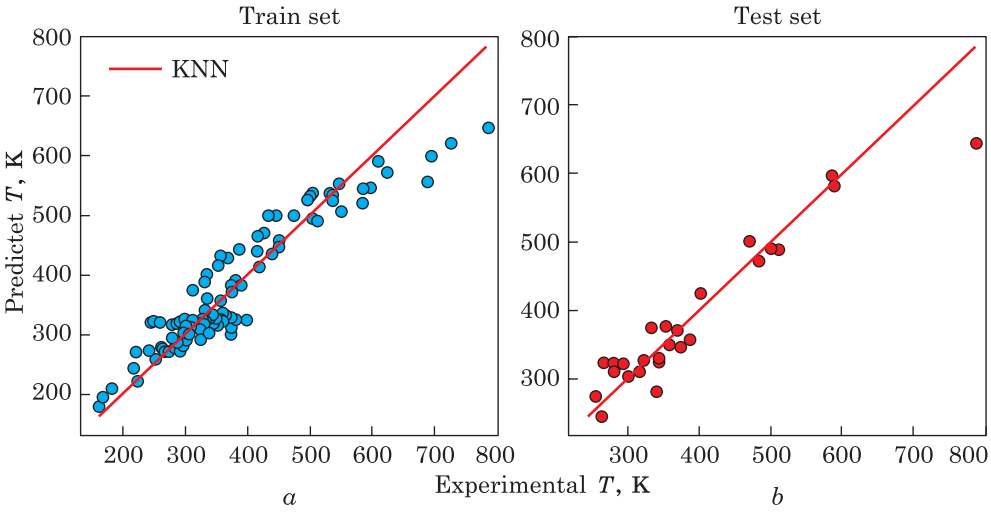

Fig. 5. Model evaluation results of KNN method

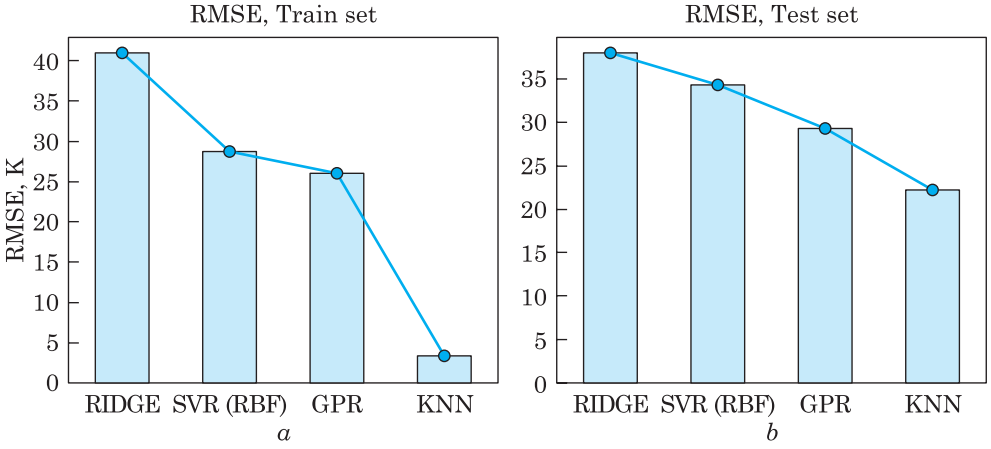

Fig. 6. RMSE results for test and train set

mance depends strongly on local neighbourhood definition rather than global model coefficients, hyperparameter optimisation focused on parameters governing local similarity structure. Specifically, the number of neighbours was optimised over the range $k \in \{2, 3, 4, 5, 7, 9, 11, 15, 20\}$, along with the neighbour weighting scheme (uniform and distance) and the distance metric (Euclidean and Manhattan), which determine how neighbouring alloy compositions influence prediction. The optimal hyperparameter configuration was selected based on cross-validation error minimisation using Mean Squared Error as the optimisation criterion. Final model performance was evaluated using RMSE and coefficient of determination R^2, confirming the robustness, accuracy, and reproducibility of the

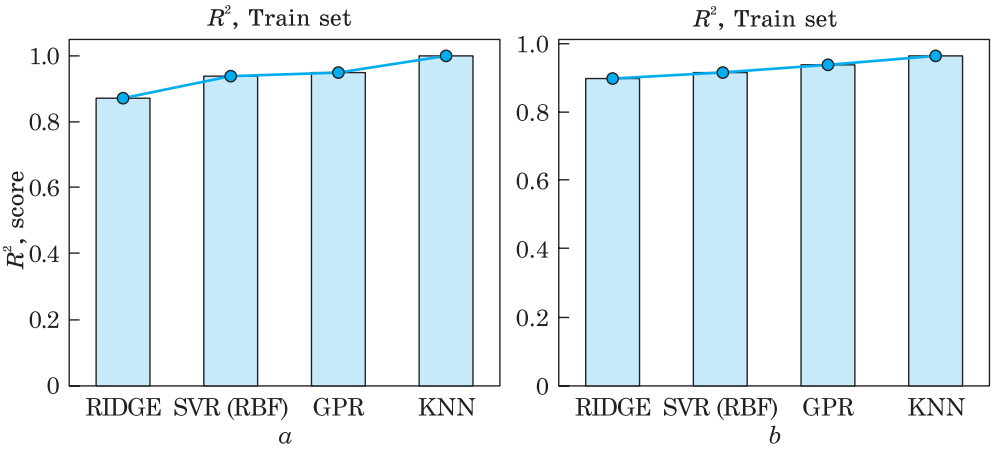

Fig. 7. R^2 results for test and train set

optimised KNN regression model. The KNN model demonstrated the highest predictive accuracy among all considered methods. The training set results showed an RMSE of 3.3654 K and an R^2 value of 0.9991 (Fig. 5, *a*), indicating an almost perfect fit to the training data. On the test set, the model achieved an RMSE of 22.2569 K and an R^2 value of 0.9645 (Fig. 5, *b*), confirming excellent generalisation performance. These results indicate that the local learning approach of KNN is highly effective for modelling the relationship between alloy composition and transformation temperature.

The comparative analysis confirms that nonlinear regression models provide substantially improved predictive performance compared to linear regression [106, 107]. The highest RMSE values are observed for ridge regression, as shown in Fig. 6, *a*, indicating its limited ability to model the complex relationships in the dataset. In contrast, SVR (RBF), GPR, and especially KNN achieve significantly lower prediction errors, with KNN demonstrating the best performance on unseen data, as illustrated in Fig. 6, *b*.

The same trend is reflected in the coefficient of determination results. Ridge exhibits the lowest explanatory capability, whereas nonlinear models achieve considerably higher accuracy. The superior fitting ability of KNN is evident from its near-perfect training performance in Fig. 7, *a*, while its strong generalisation capability is confirmed by the highest test R^2 score in Fig. 7, *b*.

Overall, these results demonstrate the necessity of nonlinear modelling for accurate prediction, with KNN providing the highest predictive accuracy and SVR (RBF) and GPR offering stable and reliable performance.

4. Conclusion

This study employed machine-learning techniques to predict the austenite finish-transformation temperature (A_f) of NiTi-based shape-memory alloys using elemental atomic compositions as input features. A dataset comprising 146 experimentally reported alloy compositions was utilised, with A_f selected as the target variable due to its critical influence on functional performance. The dataset was divided into training and testing subsets, and multiple regression models were evaluated.

The results indicate that linear approaches, such as ridge regression, exhibit limited predictive capability, reflecting the inherently nonlinear relationship between alloy composition and transformation temperature. In contrast, nonlinear models significantly enhanced prediction accuracy. Support vector regression and Gaussian process regression demonstrated strong performance, with the latter benefiting from its probabilistic framework. Among all models, *k*-nearest neighbours' regression achieved the highest accuracy and generalisation ability.

Overall, the findings confirm that A_f prediction in NiTi-based alloys requires nonlinear modelling strategies. The high predictive performance of the applied machine learning methods highlights their effectiveness as data-driven tools for accelerating alloy design and reducing experimental workload in the development of advanced shape-memory materials.

Authors' Contributions. M.M.Y. conducted a comprehensive literature review of NiTi-based shape-memory alloys presented in tabular form in the second section of the manuscript and examined their phase transformation temperatures. Ch.A.I. and L.A.G. developed appropriate algorithms in the Python 3.14 programming environment to process the data presented in Table 1, constructed the models, and visualised the results. A.H.G. carried out a systematic review of the literature presented in the first section concerning the importance of applying machine-learning methods to predict the austenite finish-transformation temperature (A_f) in NiTi-based shape-memory alloys. N.A.G. performed the literature survey, collected and analysed data obtained by other researchers, and prepared the manuscript with the contributions of all co-authors. The final version of the manuscript was critically reviewed and approved by all authors.

REFERENCES

1. G.B. Olson, *Science*, **288**: 993 (2000); https://doi.org/10.1126/science.288.5468.993
2. J.H. Panchal, S.R. Kalidindi, and D.L. McDowell, *Comput. Aided Des.*, **45**: 4 (2013); https://doi.org/10.1016/j.cad.2012.06.006
3. J. Allison, D. Backman, and L. Christodoulou, *JOM*, **58**: 25 (2006); https://doi.org/10.1007/s11837-006-0223-5
4. A.A. White, *MRS Bulletin.*, **38**: 594 (2013); https://doi.org/10.1557/mrs.2013.187

5. T.M. Pollock, *Nat. Mater.*, **15**: 809 (2016); https://doi.org/10.1038/nmat4709
6. A.D. Spear, S.R. Kalidindi, B. Meredig, A. Kontsos, and J.-B. Le Graverend, *JOM*, **70**: 1143 (2018); https://doi.org/10.1007/s11837-018-2894-0
7. J. Ling, M. Hutchinson, E. Antono, S. Paradiso, and B. Meredig, *Integr. Mater. Manuf. Innov.*, **6**: 207 (2017); https://doi.org/10.1007/s40192-017-0098-z
8. D. Xue, P.V. Balachandran, J. Hogden, J. Theiler, and T. Lookman, *Nat. Commun.*, **7**: 11241 (2016); https://doi.org/10.1038/ncomms11241
9. S. Curtarolo, G.L.W. Hart, M.B. Nardelli, N. Mingo, S. Sanvito, and O. Levy, *Nat. Mater.*, **12**: 191 (2013); https://doi.org/10.1038/nmat3568
10. S. Curtarolo, W. Setyawan, G.L.W. Hart, M. Jahnatek, R.V. Chepulskii, R.H. Taylor, S. Wang, J. Xue, K. Yang, O. Levy, M.J. Mehl, H.T. Stokes, D.O. Demchenko, and D. Morgan, *Comput. Mater. Sci.*, **58**: 2018 (2012); https://doi.org/10.1016/j.commatsci.2012.02.005
11. J.E. Saal, S. Kirklin, M. Aykol, B. Meredig, and C. Wolverton, *JOM*, **65**: 1501 (2013); https://doi.org/10.1007/s11837-013-0755-4
12. Jain, S.P. Ong, G. Hautier, W. Chen, W.D. Richards, S. Dacek, S. Cholia, D. Gunter, D. Skinner, G. Ceder, and K.A. Persson, *APL Mater.*, **1**: 011002 (2013); https://doi.org/10.1063/1.4812323
13. F. Ren, L. Ward, T. Williams, K.J. Laws, C. Wolverton, J. Hattrick-Simpers, and A. Mehta, *Sci. Adv.*, **4**, No. 4 (2018); https://doi.org/10.1126/sciadv.aaq1566
14. L. Ward, A. Agrawal, A. Choudhary, and C. Wolverton, *npj Comput. Mater.*, **2**: 16028 (2016); https://doi.org/10.1038/npjcompumats.2016.28
15. L.M. Ghiringhelli, J. Vybiral, S.V. Levchenko, C. Draxl, and M. Scheffler, *Phys. Rev. Lett.*, **114**: 105503 (2015); https://doi.org/10.1103/PhysRevLett.114.105503
16. O. Isayev, C. Oses, C. Toher, E. Gossett, S. Curtarolo, and A. Tropsha, *Nat. Commun.*, **8**: 105503 (2017); https://doi.org/10.1038/ncomms15679
17. V. Stanev, C. Oses, A.G. Kusne, E. Rodriguez, J. Paglione, S. Curtarolo, and I. Takeuchi, *npj Comput. Mater.*, **4**: 29 (2018); https://doi.org/10.1038/s41524-018-0085-8
18. B. Meredig, E. Antono, C. Church, M. Hutchinson, J. Ling, S. Paradiso, B. Blaiszik, I. Foster, B. Gibbons, J. Hattrick-Simpers, A. Mehtaf, and L. Ward, *Mol. Syst. Des. Eng.*, **3**: 819 (2018); https://doi.org/10.1039/C8ME00012C
19. A.O. Oliynyk, E. Antono, T.D. Sparks, L. Ghadbeigi, M.W. Gaultois, B. Meredig, and A. Mar, *Chem. Mater.*, **28**: 7324 (2016); https://doi.org/10.1021/acs.chemmater.6b02724
20. J. Carrete, N. Mingo, S. Wang, and S. Curtarolo, *Phys. Rev. X*, **4**: 011019 (2014); https://doi.org/10.1103/PhysRevX.4.011019
21. P.V. Balachandran, A.A. Emery, J.E. Gubernatis, T. Lookman, Ch. Wolverton, and A. Zunger, *Phys. Rev. Mater.*, **2**: 043802 (2018); https://doi.org/10.1103/PhysRevMaterials.2.043802

22. C. Oses, C. Toher, S. Curtarolo, *Nat. Rev. Mater.*, **5**: 295 (2020); https://doi.org/10.1038/s41578-019-0170-8
23. T.E. Buchheit, D.F. Susan, J.E. Massad, J.R. McElhanon, and R.D. Noebe, *Metall. Mater. Trans A*, **47**: 1587 (2016); https://doi.org/10.1007/s11661-016-3324-y
24. G.B. Olson and C.J. Kuehmann, *Scr. Mater.*, **70**: 27 (2014); https://doi.org/10.1016/j.scriptamat.2013.08.032
25. J.H. Martin, B.D. Yahata, J.M. Hundley, J.A. Mayer, T.A. Schaedler, and Tresa M. Pollock, *Nature*, **549**: 365 (2017); https://doi.org/10.1038/nature23894
26. K. Otsuka and C.M. Wayman, *Shape Memory Materials* (Cambridge Univ. Press: 1999).
27. K. Otsuka and T. Kakeshita, *MRS Bull.*, **27**: 91 (2002); https://doi.org/10.1557/mrs2002.43
28. J.S. Juan, M.L. Nó, and Ch.A. Schuh, *Nat. Nanotechnol.*, **4**: 415 (2009); https://doi.org/10.1038/nnano.2009.142
29. J.N. Aslanov, Z.S. Huseynli, and G.S. Hasanov, *Int. J. Tech. Phys. Probl. Eng.*, **17**: 446 (2025).
30. Y. Song, X. Chen, V. Dabade, T.W. Shield, and R.D. James, *Nature*, **502**: 85 (2013); https://doi.org/10.1038/nature12532
31. C. Chluba, W. Ge, R.L. de Miranda, J. Strobel, L. Kienle, E. Quandt, and M. Wuttig, *Science*, **348**: 1004 (2015); https://doi.org/10.1126/science.1261164
32. J. Cui, Y.S. Chu, O.O. Famodu, Y. Furuya, J. Hattrick-Simpers, R.D. James, A. Ludwig, S. Thienhaus, M. Wuttig, Z. Zhang, and I. Takeuchi, *Nat. Mater.*, **5**: 286 (2006); https://doi.org/10.1038/nmat1593
33. M. Zarinejad and Y. Liu, *Adv. Funct. Mater.*, **18**: 2789 (2008); https://doi.org/10.1002/adfm.200701423
34. J. Frenzel, A. Wieczorek, I. Opahle, B. Maaß, R. Drautz, and G. Eggeler, *Acta Mater.*, **90**: 213 (2015); https://doi.org/10.1016/j.actamat.2015.02.029
35. K. Otsuka and X.B. Ren, *Mater. Sci. Forum*, **394**: 177 (2002); https://doi.org/10.4028/www.scientific.net/MSF.394-395.177
36. X.B. Ren and K. Otsuka, *Mater. Sci. Forum*, **327**: 413 (2000); https://doi.org/10.4028/www.scientific.net/MSF.327-328.413
37. J. Ma, I. Karaman, and R.D. Noebe, *Int. Mater. Rev.*, **55**: 257 (2010); https://doi.org/10.1179/095066010X12646898728363
38. J. Frenzel, E.P. George, A. Dlouhy, Ch. Somsen, M.F.-X. Wagner, and G. Eggeler, *Acta Mater.*, **58**: 3444 (2010); https://doi.org/10.1016/j.actamat.2010.02.019
39. Yu.M. Koval, V.S. Filatova, V.V. Odnosum, O.A. Shcheretskyi, and G.S. Firstov, *Metallofiz. Noveishie Tekhnol.*, **47**: 1281 (2025); https://doi.org/10.15407/mfint.47.12.1281
40. G.S. Firstov, Yu.M. Koval, V.S. Filatova, V.V. Odnosum, G. Gerstein, and H.J. Maier, *Prog. Phys. Met.*, **24**: 819 (2023); https://doi.org/10.15407/ufm.24.04.819
41. J.C. Chekotu, R. Goodall, D. Kinahan, D. Brabazon, *Materials & Design,* **218**: 110715 (2022); https://doi.org/10.1016/j.matdes.2022.110715
42. N. Agarwal, J.R. Murphy, T.S. Hashemi, T. Mossop, D. O'Neill, J. Power, A. Shayegh, and D. Brabazon, *Materials*, **16**: 6480 (2023); https://doi.org/10.3390/ma16196480

43. T.C. Dzogbewu and D.J. de Beer, *Heliyon*, **10**: e23369 (2024); https://doi.org/10.1016/j.heliyon.2023.e23369
44. Y. Zhang, D. Wei, Y. Chen, L. Xie, L. Wang, L.-C. Zhang, W. Lu, and G. Chen, *J. Mater. Sci. Technol.*, **186**: 48 (2024); https://doi.org/10.1016/j.jmst.2023.10.053
45. S.W. Robertson, A. Pequegnat, E. Borgeson, K. Chapman, Ch. Fahey, and E. Veit, *Shape Memory and Superelasticity*, **11**: 669 (2025); https://doi.org/10.1007/s40830-025-00541-0
46. S. Liu, B.B. Kappes, B. Amin-ahmadi, O. Benafan, X. Zhang, and A.P. Stebner, *Appl. Mater. Today*, **22**: 100898 (2021); https://doi.org/10.1016/j.apmt.2020.100898
47. D. Xue, D. Xue, R. Yuan, Y. Zhou, P.V. Balachandran, X. Ding, J. Sun, and T. Lookman, *Acta Mater.*, **125**: 532 (2017); https://doi.org/10.1016/j.actamat.2016.12.009
48. H. Abedi, K.S. Baghbaderani, A. Alafaghani, M. Nematollahi, F. Kordizadeh, M.M. Attallah, A. Qattawi, and M. Elahinia, *J. Materi Eng and Perform.*, **31**: 10258 (2022); https://doi.org/10.1007/s11665-022-06995-y
49. S.R. Kalidindi and M. De Graef, *Annu. Rev. Mater. Res.*, **45**: 171 (2015); https://doi.org/10.1146/annurev-matsci-070214-020844
50. M.B. Babanli and K.H. Ismayilova, *11th International Conference on Theory and Application of Soft Computing, Computing with Words and Perceptions and Artificial Intelligence. Lecture Notes in Networks and Systems. Vol. **362*** (Springer: 2022), p. 459; https://doi.org/10.1007/978-3-030-92127-9_62
51. R.K. Mehtiyev and Yu.A. Tanriverdiyev, *J. Machinery Manuf. Reliability,* **54**: 586 (2025); https://doi.org/10.1134/S1052618825700955
52. P. Raccuglia, K.C. Elbert, P.D.F. Adler, C. Falk, M.B. Wenny, A. Mollo, M. Zeller, S.A. Friedler, J. Schrier, and Alexander J. Norquist, *Nature*, **533**: 73 (2016); https://doi.org/10.1038/nature17439
53. P.V. Balachandran, D. Xue, and T. Lookman, *Phys. Rev. B*, **93**: 144111 (2016); https://doi.org/10.1103/PhysRevB.93.144111
54. E.A. Guseinova and G.S. Hasanov, *Phys. Chem. Solid State*, **25**, No. 2: 333 (2024); https://doi.org/10.15330/pcss.25.2.333-337
55. K.N. Melton and O. Mercier, *Acta Metall.*, **29**: 393 (1981); https://doi.org/10.1016/0001-6160(81)90165-6
56. Yu.M. Koval, V.V. Odnosum, T.G. Sych, G.S. Mogylnyy, V.V. Burtsev, and A.Yu. Sezonenko, *Metallofiz. Noveishie Tekhnol.*, **45**, No. 11: 1293 (2023); https://doi.org/10.15407/mfint.45.11.1293
57. J. Frenzel, A. Wieczorek, I. Opahle, B. Maaß, R. Drautz, and G. Eggeler, *Acta Mater.*, **90**: 213 (2015); https://doi.org/10.1016/j.actamat.2015.02.029
58. G. Angella, B.P. Wynne, W.M. Rainforth, and J.H. Beynon, *Acta Mater.*, **53**: 1263 (2005); https://doi.org/10.1016/j.actamat.2004.10.047
59. Y.Q. Wang, Y.F. Zheng, W. Cai, and L.C. Zhao, *Scr. Mater.*, **40**: 1327 (1999); https://doi.org/10.1016/S1359-6462(99)00085-8
60. V.G. Pushin, N.N. Kuranova, A.V. Pushin, A.N. Uksusnikov, and N.I. Kourov, *Tech. Phys.*, **61**, No. 7: 1009 (2016); https://doi.org/10.1134/S1063784216070203

61. S.F. Hsieh, S.L. Chen, H.C. Lin, M.H. Lin, J.H. Huang, M.C. Lin, *J. Alloys Compd.*, **494**: 155 (2010);
https://doi.org/10.1016/j.jallcom.2010.01.052
62. S.B. Glen *et al.*, *Metall. Mater. Trans. A*, **41** (2010);
https://doi.org/10.1007/s11661-010-0257-3
63. Kh.M. Ibrahim, N. Elbagoury, and Y. Fouad, *J. Alloys Compd.*, **509**: 3913 (2007);
https://doi.org/10.1016/j.jallcom.2010.12.164
64. B. Strnadel, S. Ohashi, H. Ohtsuka, T. Ishihara, and S. Miyazaki, *Mater. Sci. Eng. A*, **202**: 148 (1995);
https://doi.org/10.1016/0921-5093(95)09801-1
65. T.E. Buchheit, D.F. Susan, J.E. Massad, J.R. McElhanon, and R.D. Noebe, *Metall. Mater. Trans. A*, **47**: 1587 (2016);
https://doi.org/10.1007/s11661-016-3324-y
66. E.A. Chyiko, X. Wang, J. Van Humbeeck, and S. Kustov, *Mater. Today: Proc.*, **4**: 4763 (2017);
https://doi.org/10.1016/j.matpr.2017.04.067
67. M.B. Babanli, *Proc. Comp. Sci.*, **120**: 104 (2017);
https://doi.org/10.1016/j.procs.2017.11.216
68. R. Coker, N. Altinkok, and A. Demir, *Mater. Des.*, **28**: 616 (2007);
https://doi.org/10.1016/j.matdes.2005.07.021
69. K.P. Mohanachandra, D. Shin, and G.P. Carman, *Smart Mater. Struct.*, **14**: S312 (2005);
https://doi.org/10.1088/0964-1726/14/5/021
70. T.H. Nam, T. Saburi, and K. Shimizu, *Mater. Trans., JIM*, **31**, No. 11: 959 (1990);
https://doi.org/10.2320/matertrans1989.31.959
71. E. Cesari, P. Ochin, R. Portier, V. Kolomytsev, Yu. Koval, A. Pasko, and V. Soolshenko, *Mater. Sci. Eng. A*, **273–275**: 738 (1999);
https://doi.org/10.1016/S0921-5093(99)00407-4
72. L. Xiao, X.Q. Zhao, F.S. Liu, and H.B. Xu, *Mater. Sci. Forum*, **546–549**: 2261 (2007);
https://doi.org/10.4028/www.scientific.net/MSF.546-549.2261
73. M. Wang, M. Jiang, G. Liao, S. Guo, and X. Zhao, *Prog. Nat. Sci.: Mater. Int.*, **22**, No. 2: 130 (2012);
https://doi.org/10.1016/j.pnsc.2012.03.010
74. K. Otsuka and X. Ren, *Intermetallics*, **7**: 511 (1999);
https://doi.org/10.1016/S0966-9795(98)00070-3
75. W. Cai, A. Liu, J. Sui, and L. Zhao, *Mater. Trans.*, **47**, No. 3: 716 (2006);
https://doi.org/10.2320/matertrans.47.716
76. J.W. Xu, A.L. Liu, B.Y. Qian, and W. Cai, *Adv. Mater. Res.*, **557–559**: 1041 (2012);
https://doi.org/10.4028/www.scientific.net/AMR.557-559.1041
77. A.L. Liu, B.T. Wu, and M.Y. Gu, *J. Mater. Sci.*, **42**: 5736 (2007);
https://doi.org/10.1007/s10853-006-0754-8
78. K.V. Ramaiah, C.N. Saikrishna, Gouthama, and S.K. Bhaumik, *Mater. Charact.*, **106**: 36 (2015);
https://doi.org/10.1016/j.matchar.2015.05.007
79. Yu.V. Kudryavtsev and E.L. Semenova, *Powder Metall. Met. Ceram.*, **48**: 700 (2009);
https://doi.org/10.1007/s11106-010-9188-6
80. M.R. Daymond, M.L. Young, J.D. Almer, D.C. DunandK.N. Melton, and O. Mercier, *Acta Metall.*, **55**: 3929 (2007);
https://doi.org/10.1016/j.actamat.2007.03.013

81. F. Cuevas, M. Latroche, P. Ochin, A. Dezellus, J.F Fernández, C. Sánchez, and A. Percheron-Guégan, *J. Alloys Compd.*, **330–332**: 250 (2002); https://doi.org/10.1016/S0925-8388(01)01636-X
82. C. Gong, F. Guo, and D. Yang, *J. Alloys Compd.*, **426**: 144 (2006); https://doi.org/10.1016/j.jallcom.2006.02.010
83. Y. Tang, Y. Wan, Z. Wang, C. Zhang, J. Han, C. Hu, and C. Tang *Mater. Des.*, **219**: 110726 (2022); https://doi.org/10.1016/j.matdes.2022.110726
84. M. Swamynathan, *Mastering Machine Learning with Python in Six Steps. A Practical Implementation Guide to Predictive Data Analytics Using Python* (Springer: 2017); https://doi.org/10.1007/978-1-4842-2866-1
85. H. Abedi, M.J. Abdollahzadeh, T. Bush, O. Benafan, A. Qattawi, and M. Elahinia, *Comput. Mater. Sci.*, **246**: 113345 (2025); https://doi.org/10.1016/j.commatsci.2024.113345
86. J.W. Xu, A.L. Liu, B.Y. Qian, and W. Cai, *Adv. Mater. Res.*, **557–559**: 10141 (2012); https://doi.org/10.4028/www.scientific.net/AMR.557-559.1041
87. V.A. Tatarenko, T.M. Radchenko, A.Yu. Naumuk, and B.M. Mordyuk, *Prog. Phys. Met.*, **25**, No. 1: 3 (2024); https://doi.org/10.15407/ufm.25.01.003
88. V.A. Tatarenko, T.M. Radchenko, A.Yu. Naumuk, and B.M. Mordyuk, *Prog. Phys. Met.*, **26**, No. 1: 3 (2025); https://doi.org/10.15407/ufm.26.01.003
89. V.A. Tatarenko and T.M. Radchenko, *Intermetallics*, **11**, Nos. 11–12: 1319 (2003); https://doi.org/10.1016/S0966-9795(03)00174-2
90. T.M. Radchenko, V.A. Tatarenko, H. Zapolsky, and D. Blavette. *J. Alloys Compd.*, **452**, No. 1: 122 (2008); https://doi.org/10.1016/j.jallcom.2006.12.149
91. T.M. Radchenko, O.S. Gatsenko, V.V. Lizunov, and V.A. Tatarenko, *Prog. Phys. Met.*, 21, No. 4: 580–618 (2020); https://doi.org/10.15407/ufm.21.04.580
92. T.M. Radchenko, O.S. Gatsenko, V.V. Lizunov, and V.A. Tatarenko, *Funda-mentals of Low-Dimensional Magnets* (Eds. R.K. Gupta, S.R. Mishra, and T.A. Nguyen) (Boca Raton: Taylor & Francis, CRC Press: 2022), Ch. 18, p. 343–364; https://doi.org/10.1201/9781003197492-18
93. V.N. Bugayev, V.G. Gavrilyuk, V.M. Nadutov, and V.A. Tatarenko, *Fizika Metallov i Metallovedenie*, **68**, No. 5: 931 (1989) (in Russian).
94. T.M. Radchenko, V.A. Tatarenko, and S.M. Bokoch, *Metallofiz. Noveishie Tekhnol.*, **28**, No. 12: 1699 (2006).
95. T.M. Radchenko and V.A. Tatarenko, *Defect Diffus. Forum*, **273–276**: 525 (2008); https://doi.org/10.4028/www.scientific.net/DDF.273-276.525
96. V.A. Tatarenko, S.M. Bokoch, V.M. Nadutov, T.M. Radchenko, and Y.B. Park, *Defect Diffus. Forum*, **280–281**: 29 (2008); https://doi.org/10.4028/www.scientific.net/DDF.280-281.29
97. L. Xiao, X.Q. Zhao, F.S. Liu, and H.B. Xu, *Mater. Sci. Forum*, **546–549**: 2261 (2007); https://doi.org/10.4028/www.scientific.net/MSF.546-549.2261
98. T.H. Nam, T. Saburi, Y. Nakata, and K. Shimizu, *Materials Transactions, JIM*, **31**: 1050 (1990); https://doi.org/10.2320/matertrans1989.31.1050

99. B. Strnadel, S. Ohashi, H. Ohtsuka, T. Ishihara, and S. Miyazaki, *Mater. Sci. Eng. A*, **202**: 148 (1995);
https://doi.org/10.1016/0921-5093(95)09801-1
100. D. Chicco, M.J. Warrens, and G. Jurman, *PeerJ Comput. Sci.*, **7**: e623 (2021);
https://doi.org/10.7717/peerj-cs.623
101. D.W. Marquardt and R.D. Snee, *Am. Stat.*, **29**, No. 1: 3 (1975);
https://doi.org/10.1080/00031305.1975.10479105
102. F. Zhou, *Data Sci. Finance Econ.*, **1**, No. 1: 1 (2021);
https://doi.org/10.3934/DSFE.2021001
103. C. Liu and H. Su, *Mater. Today Commun.*, **41**: 110720 (2024);
https://doi.org/10.1016/j.mtcomm.2024.110720
104. S.E. Saghaian, M. Hemmati, S.M. Hasan, and O. Benafan, *Int. J. Adv. Manuf. Tech.*, **13**: 6393 (2026);
https://doi.org/10.1007/s00170-026-17567-y
105. X. Tian, Y. Pan, J. Li, X. Tong, H. Li, W. Zhao, H. Zhang, and C. Tan, *J. Alloys Compd.*, **1020**: 179334 (2025);
https://doi.org/10.1016/j.jallcom.2025.179334
106. L. Thiercelin, L. Peltier, and F. Meraghni, *Computational Materials Science*, **231**: 112578 (2024);
https://doi.org/10.1016/j.commatsci.2023.112578
107. S.H. Zadeh, T.D. Brown, X. Qian, I. Karaman, and R. Arroyave, *Acta Materialia*, **289**: 120861 (2025);
https://doi.org/10.1016/j.actamat.2025.120861

Received / Final version
28.02.2026 / 02.06.2026

Н.А. Гурбанов[1], *Ч.А. Імамалізаде*[1],
Л.А. Гардашова[1], *М.М. Ясаш*[2], *А.Х. Гулієва*[3]
[1] Азербайджанський державний університет нафти та промисловості,
пр. Азадлиг, 20, Баку, Азербайджан
[2] Університет Карабюк, 413 просп., 10, 78050 Карабюк, Туреччина
[3] Бакинський інженерний університет,
Хірдалан-сіті, просп. Гасана Алієва, 120, AZ0101 Баку, Азербайджан

ДОСЛІДЖЕННЯ ВЗАЄМОЗВ'ЯЗКУ МІЖ СКЛАДОМ І ТЕМПЕРАТУРОЮ ФАЗОВОГО ПЕРЕТВОРЕННЯ СПЛАВІВ НА ОСНОВІ NiTi ІЗ ВИКОРИСТАННЯМ МАШИННОГО НАВЧАННЯ

Точне прогнозування температур фазового перетворення має вирішальне значення для проєктування й оптимізації сплавів з пам'яттю форми на основі NiTi, оскільки ці температури визначають їхні функціональні характеристики та робочі діапазони. Однак зв'язок між складом сплаву та поведінкою фазового перетворення є достатньо складним і нелінійним, що утруднює надійне прогнозування за допомогою традиційних підходів моделювання. Тому в цьому дослідженні для прогнозування кінцевої температури перетворення аустеніту на основі складу сплаву застосовано методи машинного навчання. Набір даних складається з експериментально виміряних сплавів на основі NiTi, що характеризуються елементарними атомними відсотками та відповідними температурами перетворення. Перед моделюванням проведено попередню обробку даних і стандартизацію ознак для забезпечення надійного навчання й оцінки моделі. Застосовано та систематично порівняно різні

методи регресії, зокрема ребристої регресії, регресії опорних векторів, регресії на основі гауссових процесів і на основі k-найближчих сусідів. Показано, що нелінійні методи машинного навчання значно перевершують лінійну регресію у визначенні складних композиційних залежностей, що регулюють температури перетворення. Зокрема, непараметричні та ймовірнісні моделі продемонстрували ліпшу здатність до моделювання нелінійних зв'язків та експериментальної мінливості. Результати дослідження свідчать про те, що машинне навчання забезпечує ефективну та надійну основу для прогнозування температур перетворення, виходячи виключно з параметрів складу. Розроблений підхід пропонує цінний інструмент для пришвидшення проєктування на основі даних та оптимізації новітніх сплавів з пам'яттю форми, одночасно скорочуючи експериментальні зусилля та час розроблення.

Ключові слова: сплави з пам'яттю форми, фазове перетворення, модель прогнозування, машинне навчання, Python.